

Targeting ubiquitin protein ligase E3 component N-recogin 5 in cancer cells induces a CD8⁺ T cell mediated immune response

Mei Song^{a*}, Chao Wang^{b,c*}, Huan Wang^d, Tuo Zhang ^a, Jiuqi Li^e, Robert Benezra^f, Lotfi Chouchane^g, Yin-Hao Sun^h, Xin-Gang Cui^{b*}, and Xiaojing Ma^{a,d}

^aDepartment of Microbiology and Immunology, Weill Cornell Medicine, New York, NY, USA; ^bDepartment of Urinary Surgery, Gongli Hospital, Second Military Medical University (Naval Medical University), Shanghai, China; ^cDepartment of Urology, The Affiliated Changzhou No. 2 People's Hospital of Nanjing Medical University, Changzhou, Jiangsu, China; ^dSheng Yushou Center of Cell Biology and Immunology, School of Life Sciences and Biotechnology, Shanghai Jiaotong University, Shanghai, China; ^eCollege of Biological Sciences, China Agricultural University, Beijing, China; ^fCancer Biology and Genetics Program, Sloan-Kettering Institute for Cancer Research, Memorial Sloan-Kettering Cancer Center, New York, NY, USA; ^gLaboratory of Genetic Medicine and Immunology, Weill Cornell Medicine-Qatar, Qatar Foundation, Doha, Qatar; ^hDepartment of Urology, Changhai Hospital, Second Military Medical University (Naval Medical University), Shanghai, China

ABSTRACT

UBR5 is a nuclear phosphoprotein of obscure functions. Clinical analyses reveal that *UBR5* amplifications and overexpression occur in over 20% cases of human breast cancers. Breast cancer patients carrying *UBR5* genetic lesions with overexpression have significantly reduced survival. Experimental work *in vitro* and *in vivo* demonstrates that UBR5, functioning as an oncoprotein, plays a profound role in breast cancer growth and metastasis. UBR5 drives tumor growth largely through paracrine interactions with the immune system, particularly through inhibiting the cytotoxic response mediated by CD8⁺ T lymphocytes, whereas it facilitates metastasis in a tumor cell-autonomous manner via its transcriptional control of key regulators of the epithelial-mesenchymal transition, ID1 and ID3. Furthermore, simultaneous targeting of UBR5 and PD-L1 yields strong therapeutic benefit to tumor-bearing hosts. This work significantly expands our scarce understanding of the pathophysiology and immunobiology of a fundamentally important molecule and has strong implications for the development of novel immunotherapy to treat highly aggressive breast cancers that resist conventional treatment.

ARTICLE HISTORY

Received 8 August 2019
Revised 16 December 2019
Accepted 4 January 2020

KEYWORDS

UBR5; E3 ligase; breast cancer; metastasis; immunotherapy

Introduction

Breast cancer is the most common malignancy among women in the United States and the second most common cause of mortality among women ages 45 to 55 y.¹ Estimated 249,260 new breast cancer cases were identified in the United States in 2016 and the predicted number of deaths is that year was 40,890.¹ Despite the development of newer diagnostic methods, selective as well as targeted chemotherapies and their combinations, surgery, hormonal therapy, radiotherapy, breast cancer recurrence, metastasis, and drug resistance are still the major problems for breast cancer. Clearly, more therapeutic modalities are needed for this most common form of cancer diagnosed in women worldwide. In an effort to identify potential “driver” genetic alterations for human breast cancer development and/or pathogenesis, we analyzed the whole-exon sequence data from the surgical tumor samples of a cohort of triple-negative breast cancer (TNBC) patients in comparison to the surrounding normal tissues.² One of the most strikingly altered genes in over 30% of the specimens that we examined was ubiquitin protein ligase E3

component n-recogin 5 (UBR5, *a.k.a.*, EDD), a member of the rare HECT-domain E3 ubiquitin ligase family.³

The biology of UBR5 is poorly understood. UBR5 is highly conserved in metazoans and is essential for early embryonic development in mice,^{4,5} indicating its fundamental importance. A recent report demonstrates that UBR5 ubiquitylates CSPP1, a centrosomal and ciliary protein involved in cilia formation, and is required for cytoplasmic organization of CSPP1-comprising centriolar satellites in the centrosomal periphery, suggesting that UBR5-mediated ubiquitylation of CSPP1 or associated centriolar satellite constituents is one underlying requirement for cilia expression.⁶ Another report indicates that as a modulator of super-vigilant proteostasis UBR5 suppresses proteostasis collapse in pluripotent stem cells from Huntington's disease patients.⁷ Human *UBR5* was originally identified in a screen for progesterin-regulated genes in breast cancer cells.³ It is rarely mutated in healthy somatic tissues but is mutated and overexpressed in many major cancers.⁸ However, the causality, activities, and mechanisms of UBR5's tumorigenic activities and the associated genetic lesions had not been established. Through genetic, cellular,

CONTACT Xiaojing Ma  xim2002@med.cornell.edu  cuixingang@smmu.edu.cn  superwang2012@aliyun.com

*These authors contributed equally to this work.

 Supplemental data for this article can be accessed on the [publisher's website](#).

© 2020 The Author(s). Published with license by Taylor & Francis Group, LLC.

This is an Open Access article distributed under the terms of the Creative Commons Attribution-NonCommercial License (<http://creativecommons.org/licenses/by-nc/4.0/>), which permits unrestricted non-commercial use, distribution, and reproduction in any medium, provided the original work is properly cited.

and molecular manipulations in mouse models, we first uncovered a distinctive and profound role of UBR5 in the aggression of an experimental TNBC model.² Further, we found that UBR5's tumorigenic activities are exerted paracrine mainly through its interaction with the adaptive immune apparatus, whereas its metastasis-promoting property is purely "cell-intrinsic", independent of the immune system and even of UBR5's E3 ubiquitin ligase activity.² In the present study, we further explored the cellular and molecular mechanisms whereby UBR5 drives tumor growth and metastasis, and the potential of UBR5 as a novel immunotherapeutic target for aggressive breast cancer.

Materials and methods

Cell cultures

4T1 cell line (CRL-2539) was obtained from ATCC in 2012. 4T1 cells were cultured in RPMI-1640 supplemented with 10% fetal bovine serum, 2 mM glutamine, 100 U/mL Penicillin and 100 µg/mL Streptomycin at 37°C in a humidified atmosphere of 5% CO₂. Cells were split when they reached 80%-90% confluence. For all experiments, cells were grown to 80%-90% confluence before experimentation.

Human breast cancer cell MCF-7 was cultured in DMEM with 10% fetal bovine serum, 2 mM glutamine, 100 U/mL Penicillin, and 100 µg/mL Streptomycin. For RNAi-mediated UBR5/EDD expression silencing, cells were transfected with 20 µmol/L of *Ubr5*-siRNA duplex (5'-CAACUUAGAUCUCCUGAAA-3') and Lipofectamine RNAiMAX (Invitrogen, 13778075) as per the manufacturer's instructions. Nonspecific siRNA oligo (Sigma, SIC002) was used as a negative control.

To generate UBR5-reconstituted 4T1/*Ubr5*^{-/-} cell line, cells were transfected with pCMV-Tag2B EDD1 (Addgene, #37188) using lipofectamine 3000 (Invitrogen, L3000008) as per the manufacturer's protocol. To generate *Id1* or *Id1/Id3* reconstituted cell lines in 4T1/*Ubr5*^{-/-}, cells were transfected with pCMV3-*Id1* (provided by Dr. Robert Benezra), pEF1α-IRES-*Id1/Id3* using lipofectamine 3000, respectively. All stable cell lines were selected with G418 and confirmed by q-PCR and western blot.

To knockdown *Raet1e* expression in 4T1/*Ubr5*^{-/-}, cells were transfected with 20 µmol/L of *Raet1e*-siRNA duplex (ThermoFisher, AM16708) and Lipofectamine RNAiMAX (Invitrogen, 13778075) as per the manufacturer's instructions. Nonspecific siRNA oligo (Sigma, SIC002) was used as a negative control. Forty-eight hour post-siRNA transfection, cells were harvested for knocking down efficiency evaluation and mice injection.

Mice and tumor model

Female BALB/c mice aged 6–8 weeks were purchased from Jackson Laboratory. To induce the 4T1 orthotopic mammary tumor, 5 × 10⁵ 4T1 cells were injected subcutaneously (s.c.) in the abdominal mammary gland and mice were euthanized at indicated times for analysis or monitored for survival. The volume of tumors was calculated as $V = L \times W^2/2$, where L and W stand for tumor length and width, respectively. For the

lung metastasis model of 4T1, 2 × 10⁵ cells were intravenously infused through the tail vein and mice were sacrificed on d 18 for analysis. For T cell depletion, 4T1 tumor-bearing mice were given anti-mouse CD8α antibody (100 µg/mouse, Clone 2.43, BioXcell) or anti-mouse CD4 antibody (250 µg/mouse, Clone GK1.5, BioXcell) at indicated times. All animal experiments were performed in accordance with National Institutes of Health guidelines for housing and care of laboratory animals after protocol (protocol Number 0701-569A) approved by IACUC at Weill Cornell Medicine.

Cell proliferation assay

Cell proliferation was evaluated by Sulforhodamine B (SRB) assay. Briefly, cells (1 × 10⁴/well) were seeded into 96 well plates and cultured for 24 h, 48 h, and 72 h, then fixed with 10% trichloroacetic acid (Sigma, T8657) for 30 min at 4°C and stained with 0.4% (w/v) SRB (Sigma, 230162) in 1% acetic acid solution for 30 min. After washing with 1% acetic acid, bound SRB was solubilized with 10 mmol/L Tris buffer, and absorbance (OD) was measured at 510 nm using 96 well plate reader.

RNA isolation and qRT-PCR

Total RNAs were extracted with the RNeasy Plus Mini Kit (QIAGEN, 74134), and cDNA was synthesized using the High Capacity cDNA Reverse Transcription Kit (Applied Biosystem, 4368814). Quantitative PCR was performed on QuantStudioTM 6 Flex System (Applied Biosystem) using PowerUp SYBR Green Master Mix (Thermo Fisher). RT-PCR primers for *Id1*: CCCAGAACCGCAAAGTGAGC (forward), CGGTGGTCCCCACTTCAGAC (reverse); for *Id3*: CGACCGAGGAGCCTCTTAGC (forward), ACGCTGCA GGATTTCCACCT (reverse); for *Gapdh*: GTCCTTCCTG GCCTAGAGGT (forward), GATGCAGGGATGATGTTCTG (reverse). The expression levels of target genes were normalized with *Gapdh* abundance. Data were presented as the average of triplicates ± SD.

Western blot

Cells were lysed in RIPA buffer (Thermal Scientific) and the lysates were centrifuged at 12,000 × rpm for 30 min at 4°C. Supernatants were collected and protein concentration was quantified by Bio-rad protein assay (Bio-rad, 5000006). Cell lysates were subjected to SDS-PAGE and transected to the PVDF membrane, followed by immunoblotting with antibodies against UBR5 (NBP2-1591, Novus Biologicals), E-cadherin (NBP2-19051, Novus Biologicals), ID1 (195–14, CalBioReagents), ID3 (16–1, CalBioReagents), *Raet1e* (ab95202, Abcam), and GAPDH (sc-FL335, Santa Cruz).

Clonogenic assays

4T1 cells were seeded in 6-well plates (100 cells/well) and cultured at 37°C in a humidified atmosphere of 5% CO₂. After 10 d, cells were washed with PBS and fixed with 4% paraformaldehyde and then stained with 0.5% crystal violet.

The number of colonies formed in each well was counted and photographed under the microscope. All assays were performed in triplicate.

Flow cytometry

Primary tumor tissues were harvested, weighed, and digested with tissue dissociation buffer [~ 280 U/mL Collagenase Type3, 4 μ g/mL DNase in HBSS] for 1 h in 37°C water bath with periodic vortexing and mashed through 70 μ m filters, layered on a 44% and 66% Percoll gradient (GE), and centrifuged at 3000 rpm for 30 min without brake. After 20 min incubation with Zombie UV™ Fixable stain at room temperature, all samples were washed with BD FACS buffer and stained with the appropriate surface antibodies. CD3 (17A2), CD8 α (53–6.7), NK1.1 (PK136), CD11b (M1/70), F4/80 (BM8), Gr-1 (RB6-8C5), Ly6 G-PE (Clone 1A8), Ly6 C-PEcy7 (Clone HK1.4), MHCII (Clone CD11 c (N418), MHCI (M5/114.15.2) were purchased from Biolegend. CD45 (30-F11), CD4 (GK1.5), CD25 (PC61.5), and Foxp3 (FJK-16 s) were purchased from eBioscience. All antibodies were tested with their isotype controls. Intracellular staining for Foxp3 and Granzyme B was performed according to Foxp3/Transcription Factor Staining buffer set (eBioscience). Data acquisition was performed on FACSCalibur (BC Biosciences) and analyzed via FlowJo.

Invasion transwell assay

The Transwell assay was performed as previously described.² Briefly, 2×10^4 4T1 cells overnight cultured in serum-free medium were seeded onto Matrigel bedding Chambers (24-well, 356234, Corning) with serum-free medium. After 24 h incubation, migrated cells determined and quantified.

Bioinformatic analysis of UBR5 mRNA expression in breast cancer patients' specimens and survival

The bioinformatic analysis of breast cancer patients was based on the data from The Cancer Genome Atlas (TCGA) project and MET500 dataset.⁹ UBR5 mRNA expression data was retrieved based on RNA-seq assay from Firehose (<http://gdac.broadinstitute.org/>). Analysis of UBR5 mRNA expression was based on UALCAN.¹⁰ The clinical survival data of breast cancer patients in TCGA was retrieved according to the pipeline of <https://portal.gdc.cancer.gov> and Liu.¹¹ Kaplan–Meier analysis of percent survival was performed with R version 3.4.4 (<https://www.r-project.org/about.html>).

RNA-seq analysis

cDNA libraries were made using the Illumina TruSeq Stranded mRNA Library Prep kit and were sequenced with single-end 51 bps on Illumina HiSeq4000 instrument. STAR¹² was used to align raw sequencing reads to the mouse GRCm38 reference genome. Raw read counts were calculated using HTseq-count.¹³ Differential expression analysis was performed using the DESeq2 package.¹⁴ We selected 1269

differentially expressed genes with adjusted p -value $< 1e-10$ and log2 FoldChange greater than 2.0 (up-regulated) or smaller than -2.0 (down-regulated), for pathway analysis using the Ingenuity Pathway Analysis (IPA).¹⁵

LC-MS and data analysis

A Thermo Fisher Scientific EASY-nLC 1000 coupled on-line to a Fusion Lumos mass spectrometer (Thermo Fisher Scientific) was used. Buffer A (0.1% FA in water) and buffer B (0.1% FA in 100% ACN) were used as mobile phases for gradient separation. A 75 μ m x 15 cm chromatography column (ReproSil-Pur C18-AQ, 3 μ m, Dr. Maisch GmbH, German) was packed in-house for peptides separation. Peptides were separated with a gradient of 5–30% buffer B over 220 min, 30%–80% B over 20 min at a flow rate of 300 nL/min. The Fusion Lumos mass spectrometer was operated in data-dependent mode. Full MS scans were acquired in the Orbitrap mass analyzer over a range of 300–1500 m/z with resolution 120,000 at m/z 200. Up to the top 20, most abundant precursors were selected with an isolation window of 0.4 Thomson and fragmented by higher-energy collisional dissociation with normalized collision energy of 40. MS/MS scans were acquired in the Orbitrap mass analyzer with resolution 30000 at m/z 200. The automatic gain control target value was $1E^6$ for full scans and $1E^5$ for MS/MS scans, respectively, and the maximum ion injection time is 60 ms for both.

The raw files were processed by using the MaxQuant computational proteomics platform (version 1.5.5.1). The fragmentation spectra were searched against the UniProt mouse protein database and allowed up to two missed tryptic cleavages. Oxidation of methionine and protein N-terminal acetylation were used as variable modifications for database searching. Carbamidomethyl cysteine was used as fixed modification. The precursor and fragment mass tolerances were set to 7 and 20 ppm, respectively. Both peptide and protein identifications were filtered at 1% false discovery rate (FDR).

Lentivirus generation and transduction

Lentiviruses were produced by co-transfection of 293 T cells with psPAX2, pMDG2, and UBR5 MISSION shRNA (TRCN0000238583, sigma) with lipofectamine 3000 (Life Technology). Virus supernatants collected 48-h and 72-h post-transfection were combined, centrifuged at 2000rpm for 10 min to remove cellular debris. Lentiviral supernatants were sterilized with 0.45 μ m pore filters. 4T1 cells were transduced with UBR5-shRNA containing lentivirus using 10 μ g/ml polybrene (Santa Cruz) and treated with 2 μ g/ml puromycin after 48 h.

Histological analysis

For paraffin-embedded tissue, organs were fixed in 4% formaldehyde overnight at 4°C. Fixed sections were then made from paraffin-embedded tissue blocks. To score tumor nodules in lung, tissue blocks were sectioned and stained

with hematoxylin/eosin (H&E) according to the manufacturer's instruction. Four to Five fields were selected from whole lung sections for five mice and all histological quantifications are presented as the mean of different tumor nodules for each individual mouse. Anti-UBR5 (Santa Cruz, sc-9562) and anti-PD-L1 (Thermo Fisher, PA5-20343) antibodies were used for immunohistochemistry, and tumor tissue sections were dewaxed in xylene and rehydrated with distilled water. After antigen unmasking with citric antigen retrieval buffer, blocking step was performed, followed by 1 h incubation at 37°C with the primary antibodies. Slides were counterstained with hematoxylin, dehydration, and mounting.

Statistics

Data are shown as mean \pm S.E.M. All experiments were repeated at least two times and results were similar between repeats. Animal experiments used between three to six mice

per group. All statistical analyses were performed using Graph Pad Prism 5.0 software. Differences between experimental groups were calculated using a two-tailed unpaired Student's t-test. Survival rates were compared using the log-rank test.

Results

UBR5 gene amplification and overexpression occur frequently in human breast cancers

Ubiquitin protein ligase E3 component n-recognin 5 (*UBR5*, a.k.a., EDD) encodes a 309 nuclear protein. Using a pooled shRNA screen to interrogate death receptor signaling, Dompe et al. identified *UBR5* along with 15 others as having the property to modulate the sensitivity to ligand-induced apoptosis, and also exhibiting frequent overexpression and/or copy number gain in human breast, pancreas, and lung cancers.¹⁶

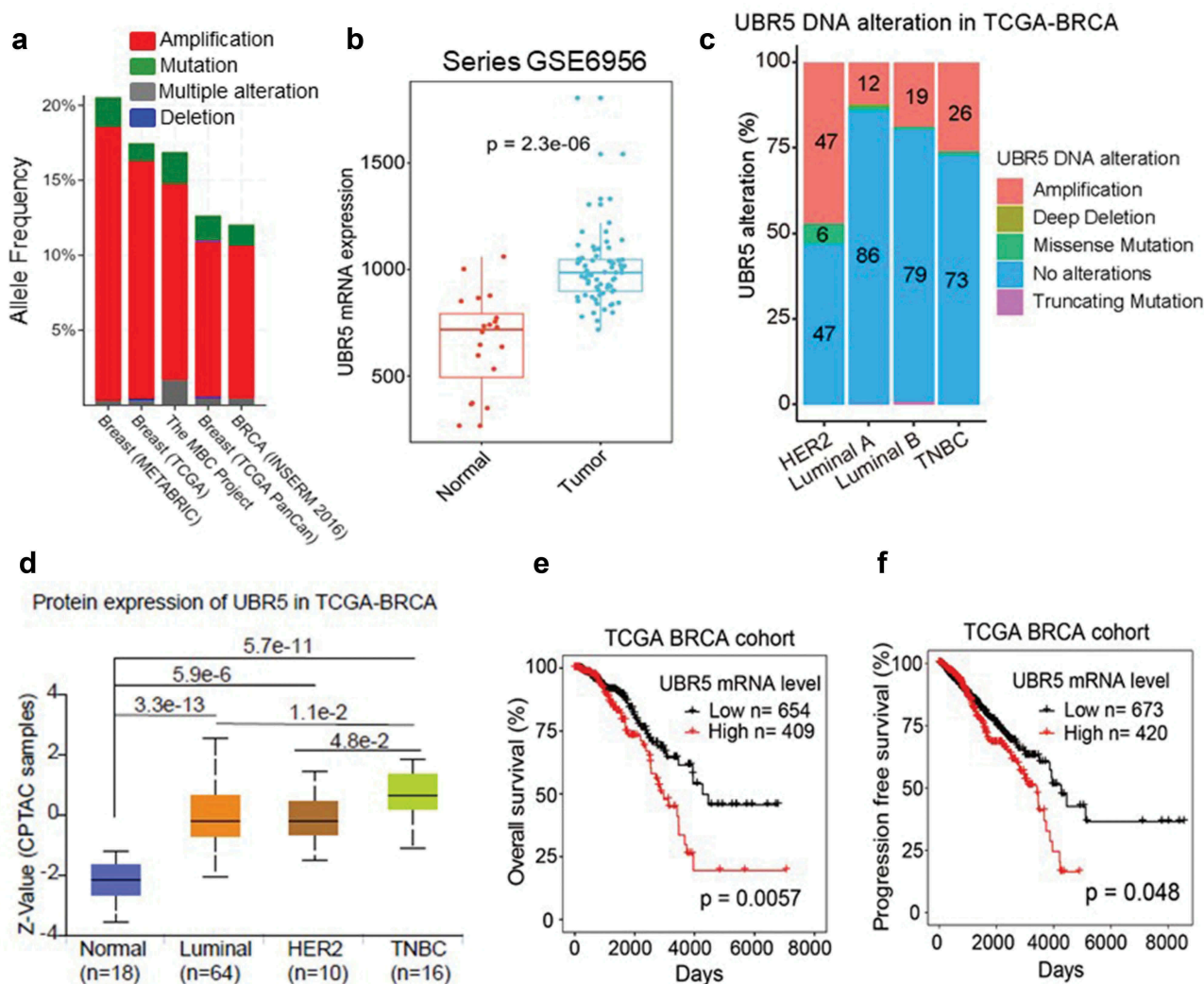


Figure 1. Meta-analysis of *UBR5*'s involvement in human breast cancers. (a) Analysis of *UBR5* gene alterations in human breast cancer studies based on the data of The Cancer Genome Atlas (TCGA) project. (b) *UBR5* mRNA level in breast cancer specimens compared to normal breast tissues (TCGA). (c) *UBR5* gene alterations in breast cancer subtypes as percentages. (d) *UBR5* protein expression in subtypes of breast cancer. (e) Correlation of *UBR5* expression with overall survival of breast cancer patients. (f) Correlation of *UBR5* expression with progression-free survival.

In a TCGA-based meta-analysis involving five independent studies and 5,151 breast cancer samples, we found that human *UBR5* gene alterations (predominantly amplifications) occur in 1221% of breast cancer cases (Figure 1a). Consistent with the gene amplification, *UBR5* mRNA expression levels in breast cancer tissues were significantly higher than in normal breast tissues (Figure 1b). Further analysis revealed that *UBR5* alterations, principally amplifications, occur in all subtypes of breast cancer to varying degrees with greatest frequency in Her2⁺ subtype (Figure 1c). Consistent with this observation, *UBR5* protein expression was significantly higher in all subtypes of breast cancer than that in normal breast tissues (Figure 1d). In addition, high *UBR5* expression positively correlates with the overall survival of breast cancer patients ($P = .0057$) (Figure 1e), as well as progression-free survival ($P = .048$) (Figure 1f). Nevertheless, very little was known about the causality, the activities, and mechanisms of *UBR5* in promoting tumor growth and metastasis, particularly *in vivo*. We undertook a series of experimental approaches through genetic, cellular, and molecular manipulations in a highly aggressive 4T1 experimental murine mammary TNBC model.

Ubr5-deletion in tumors triggers a more robust T-cell response

We explored *UBR5* functionally in the syngeneic and highly metastatic murine TNBC model, 4T1, which expresses high levels of *UBR5*. We “knocked out” *UBR5* expression in tumor cells by CRISPR/Cas9, designated 4T1/*Ubr5*^{-/-}. The efficiency of the knock out was confirmed at genomic, mRNA and protein levels.² We randomly selected three independent *Ubr5*^{-/-} clones, which displayed very similar *in vitro* propagation capacities to that of control 4T1 (Figure S1A-B). To understand the broad impact of *Ubr5* deletion on gene expression in 4T1 cells, we performed transcriptome analysis by RNA-seq comparing the three *Ubr5*^{-/-} clones with three WT GFP clones. The reproducibility of the clones was validated (Fig S2A). Hierarchical cluster analysis revealed two strikingly opposite gene expression groups between WT and *Ubr5*^{-/-} 4T1 cells (Figure S2B). Ingenuity Pathway analysis (IPA) of the combined data showed that compared to WT controls, signaling pathways involved in epithelial to mesenchymal transition (EMT) and extracellular matrix degradation as well as immune co-stimulation were up-regulated (positive z-score) in *Ubr5*^{-/-} cells, whereas STAT3-, TGF-β-, P38MAPK- and endothelin signaling pathways were downregulated (negative z-score), implying lower malignant potential and tumorigenicity of 4T1/*Ubr5*^{-/-} compared to the WT control (Figure 2a).

To assess the effects of *Ubr5* deletion on tumor growth and metastasis, female BALB/c mice (syngeneic with 4T1 tumor) were inoculated in the abdominal mammary gland with control GFP⁺ or *Ubr5*^{-/-} tumors. However, *Ubr5*^{-/-} tumor growth *in vivo* was very much arrested from d 10 onwards, and the tumors shrank gradually over time and some even disappeared completely 3 weeks after tumor cell inoculation (Figure 2b, Figure S1 C).

To further elucidate the immune mechanisms involved in the antitumor effect of *Ubr5* depletion, we analyzed the major subsets of leukocytes in the tumor microenvironment (TME),

spleen, and tumor-draining lymph nodes (TDLNs) of 4T1 bearing mice on d 11 post-tumor inoculation at which time the 4T1/*Ubr5*^{-/-} tumor started to shrink (Figure 2b). The proportion of tumor-infiltrating CD4⁺ (Figure 2c) and CD8⁺ (Figure 2d) T cells was increased by approximately twofold in 4T1/*Ubr5*^{-/-} bearing mice, compared with mice bearing control tumors. Furthermore, infiltrating CD8⁺ T cells exhibited enhanced granzyme B expression (Figure 2e), indicating a more active cytolytic state of the CD8⁺ T cells in mice carrying the *Ubr5*-deleted tumor. Although there was no significant difference in tumor-infiltrating Foxp3⁺ CD25⁺ Tregs in both types of hosts (data not shown), decreased Tregs were observed in TDLNs of 4T1/*Ubr5*^{-/-} bearing mice (Figure 2f). Populations of intra-tumoral CD3⁻NKp46⁺ NK cells (Figure S2A), CD11b⁺Ly6 C⁺/Ly6 G⁺ MDSCs (Figure S2B), and CD11 c⁺MHCII⁺ DCs (Figure S2 C) were not significantly altered between these two types of 4T1 bearing mice. Similar results were obtained in spleens, with a higher frequency of both CD4⁺ and CD8⁺ T cells in 4T1/*Ubr5*^{-/-} bearing mice (Figure S2D-G). Together, these results demonstrate that targeting *UBR5* in tumors induces a heightened immune active state of the T lymphocytes.

CD8⁺ T cell-dependent immunity is essential for controlling Ubr5^{-/-} tumor growth

To determine whether and which type of T cells control 4T1/*Ubr5*^{-/-} tumor growth, we devised a scheme to deplete CD4⁺ and CD8⁺ T cells in 4T1 tumor-bearing mice with antibodies (Figure 3a). Although both CD4⁺ and CD8⁺ T cells were markedly depleted in spleens, peritoneal cavity, and tumors as evaluated on d 21 post-tumor inoculation (Figure S4 and S5), only depletion of CD8⁺ T, not CD4⁺ T cells, caused a complete reversal of the tumor growth of 4T1/*Ubr5*^{-/-} to and above the WT tumor (Figure 3b,c), and animal survival (Figure 3d,e). In addition, lung metastasis of 4T1/*Ubr5*^{-/-} tumors was partially rescued by CD8⁺ T cell depletion but not by CD4⁺ T cell depletion (Figure 3f,h). Taken together, these data suggest that *UBR5* promotes tumor growth in a manner that is solely dependent on restricting the activities of CD8⁺ T cells.

Ubr5 deletion causes dysregulated epithelial–mesenchymal transition and impaired tumor metastasis

We previously observed that the morphology of 4T1/*Ubr5*^{-/-} was altered from a cuboidal epithelial shape, to a more elongated “mesenchymal” shape, characteristic of epithelial–mesenchymal transition (EMT).² 4T1/*Ubr5*^{-/-} cells displayed strongly reduced levels of E-cadherin, ID1 and ID3 proteins (Figure 4a), the latter two of which are critical regulators of mesenchymal–epithelial transition (MET) in metastatic colonization.¹⁷ The defects in ID1 and ID3 protein expression were also observed at the mRNA level (Figure 4b), indicating that *UBR5* regulates directly or indirectly the transcription of *Id1* and *Id3* genes. Notably, the protein expression of ID1/ID3 was completely restored to the control (4T1/GFP) level in both human EDD-reconstituted- and catalytic mutant EDD-C2768A-reconstituted- 4T1/*Ubr5*^{-/-} cells, suggesting that *UBR5* regulates ID1/ID3 expression independent

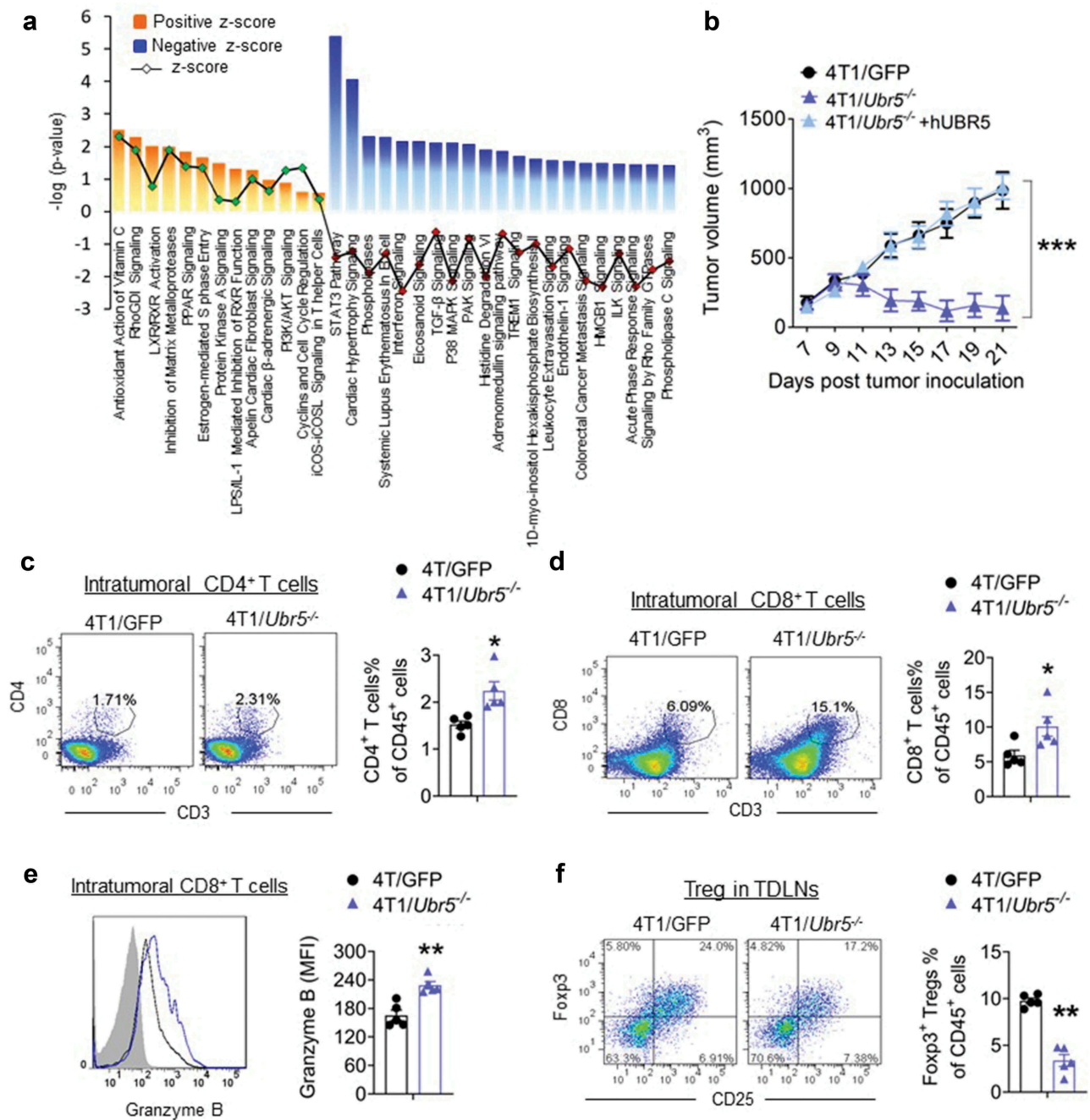


Figure 2. Immunological alterations in mice carrying *Ubr5*^{-/-} tumor. 4T1 tumor cells were s.c. injected into the mammary pad of BALB/c mice and on d 11, tumor-bearing mice were sacrificed and tumor organs were harvested for FACS analysis. (a) 4T1 tumor growth curve. Around d11, 4T1/*Ubr5*^{-/-} tumor started to shrink. (b) RNA-seq analysis of WT vs *Ubr5*^{-/-} tumors isolated on d 11. The activation states of various biological pathways are indicated. The dotted line represents the statistical significance threshold ($p < .05$). (c,d) Increased tumor-infiltrating CD4⁺/CD8⁺ T cells in 4T1/*Ubr5*^{-/-} tumor-bearing mice. (c) Representative FACS images and quantification of intratumoral CD4⁺ T cells. (d) Representative FACS images and quantification of intratumoral CD8⁺ T cells. (e) Decreased proportion of Tregs in TDLNs of 4T1/*Ubr5*^{-/-} tumor-bearing mice. Representative FACS images of Tregs in TDLNs and the quantification of Tregs in TDLN. In all cases, data are representative of at least three independent experiments using three to five mice per group. Data represent mean \pm SEM; * $P < .05$, ** $P < .01$.

of its E3 ubiquitin ligase activity (Figure 4c). In addition, the defective E-cadherin expression was also observed in UBR5-deficient human breast cancer cell line MCF-7 (Figure 4a). Reconstitution of 4T1/*Ubr5*^{-/-} cells with ID1 and ID3 together (Figure 4d), but not with ID1 alone (Figure. S7) restored their epithelial phenotype to that of the wild type 4T1 cells (Figure 4e) and reduced 4T1/*Ubr5*^{-/-} tumor cells' ability to migrate *in vitro*, measured by transwell assay, to that of the WT cells (Figure 4f,g).

The reconstitution also restored 4T1/*Ubr5*^{-/-} tumor cells' clonogenicity to the WT level (Figure 4h,i), and completely rescued the impaired lung metastasis of 4T1/*Ubr5*^{-/-} tumors *in vivo* without any difference in *in vitro* propagation capacity (Figure 4j,k, Figure S1D). These data demonstrate that UBR5 promotes tumor metastasis primarily through its transcriptional control of the major EMT regulators ID1 and ID3 in a cell-intrinsic manner.

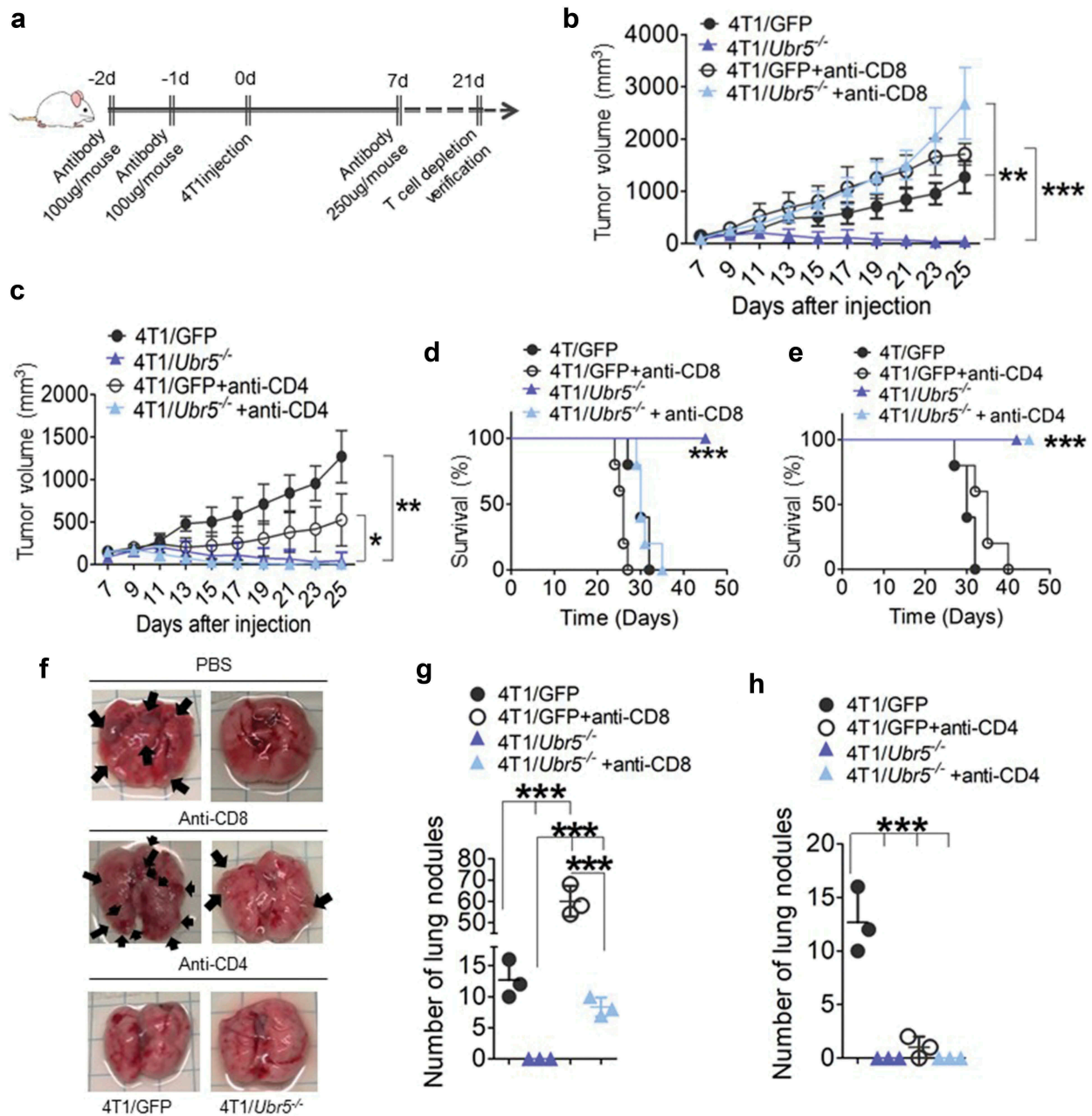


Figure 3. Effects of T cell depletion on tumor growth and metastasis. (a) Schematic for T cell depletion in 4T1 tumor-bearing mice. (bc) 4T1 tumor growth curves with CD8 T cell depletion (b) or CD4 T cell depletion (c) ($n = 5$ per group). (d,e) The survival rates of 4T1 tumor-bearing mice with CD8 T cell depletion (d) or CD4 T cell depletion (e) were monitored and quantified ($n = 5$ per group). (f,h) Lung metastasis in mice bearing 4T1 on d 24 post-tumor cells s.c. injection. (f) Representative images for lung nodules. Lung nodules in CD8 T cell-depleted tumor-bearing mice (g) and CD4 T cell-depleted tumor-bearing mice (h) were quantified. Data are representative of three independent experiments with similar results. Data represent mean \pm SEM; * $P < .05$, ** $P < .01$, *** $P < .001$.

Targeting *UBR5* may lead to induction of immunogens

We were interested in identifying *UBR5*'s substrates and direct targets. To begin such a search effort, we compared protein expression between WT and *Ubr5*^{-/-} 4T1 tumor cells by LC/MS. Out of more than 4,300 proteins identified and analyzed, 30 of them were significantly upregulated in *Ubr5*^{-/-} cells over WT cells (Table 1), whereas 33 proteins were downregulated (Figure S8). One of the upregulated proteins, Rael1e, belong to a family of ligands for NKG2D activating receptor of human natural killer (NK) cells. It has been shown to function as a ligand for both TCR $\gamma\delta_2$ and NKG2D through which Rael1e induces T

cell-mediated cytotoxicity to tumor cells.¹⁸ Decreased Rael1e expression is a poor prognostic marker in nasopharyngeal carcinoma,¹⁹ whereas high expression of Rael1e is an indicator of good prognosis in cervical cancer.²⁰ We first confirmed the MS finding of Rael1e's overexpression by Western blot in WT and in *Ubr5*^{-/-} cells treated with the proteasome inhibitor MG132 (Figure 5a), which also indicated that Rael1e protein level was indeed regulated by a proteasome-mediated mechanism. We then transiently knocked down the expression of Rael1e via siRNA in *Ubr5*^{-/-} 4T1 tumor (Figure 5b), which, when implanted in mice, caused a partial reversal of the inhibited

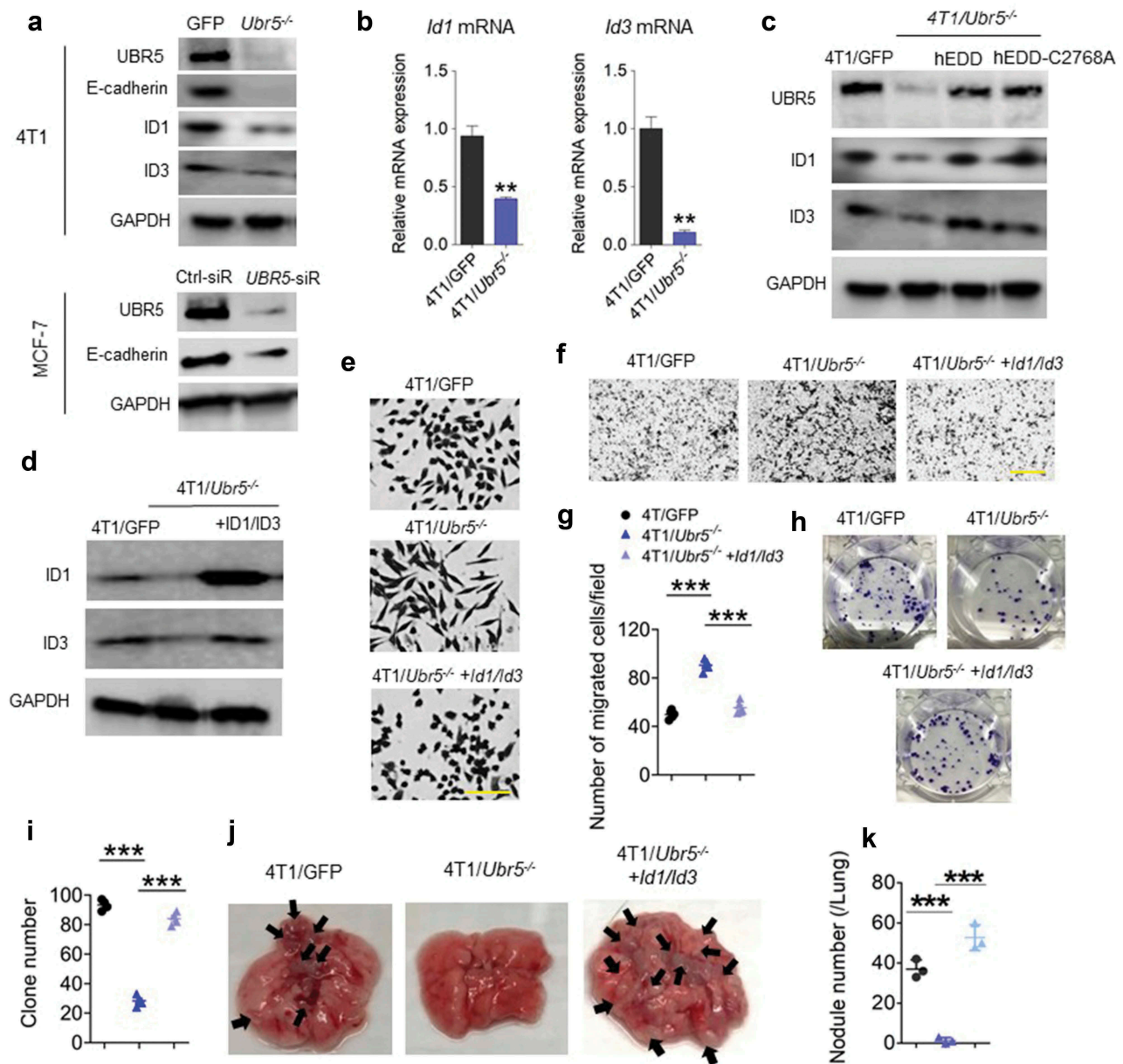


Figure 4. Effects of Ubr5 deletion on tumor metastasis. (a) Protein expression of murine UBR5, E-cadherin, ID1 and ID3 in 4T1 cells, and human E-cadherin in MCF-7 after UBR5 depletion by siRNA was evaluated by western blot. (b) Messenger RNA expression of Id1 and Id3 in 4T1 cells was assessed by qRT-PCR. (c) ID1 and ID3 protein expression in human EDD-reconstituted and catalytic mutant EDD-C2768A-reconstituted 4T1/Ubr5^{-/-} cells was evaluated by western blot. (d) Murine ID1 and ID3 reconstitution in 4T1/Ubr5^{-/-} cells were verified by western blot. (e) Representative micrographs of cell morphology of 4T1/GFP, 4T1/Ubr5^{-/-}, and 4T1/Ubr5^{-/-} + ID1/ID3 reconstituted cells in culture. Scale bars: 100 μ m. (f,g) Representative micrographs (f) and the quantification (g) of a Transwell invasion assay. (h) Representative images (h) and quantified values (i) of clonogenic assay with 100 cells/well. (j-k) 5 \times 10⁵ cells were i.v. injected into BALB/c mice and the lungs of the recipient mice were harvested on d 18. Representative images (j) and quantified values of metastatic nodules in lung (k) ($n = 3$ per group). Data are representative of two independent experiments with similar results. Data represent mean \pm SEM, ** $P < .01$, *** $P < .001$.

growth of the parental tumor (Figure 5c), but did not alter the *in vitro* growth rates (Figure S1E), suggesting that higher Rael1e expression may mediate an adverse response against the tumor and that UBR5 deficiency in tumor cells may generate immunogens that attract anti-tumor responses.

Dual targeting of UBR5 and PD-L1 yields superior therapeutic benefits

UBR5 is an important regulator of genome stability through its modulation of the activity of the DNA damage checkpoint

kinase, CHK2,²¹ its control of p53 levels²² and ATM-mediated phosphorylation of p53.²³ We hypothesize that UBR5 deletion may result in genome instability and mutagenesis, inducing potential neoantigens which will attract T cell-mediated tumor-specific responses. We observed that Ubr5-deletion did not affect PD-L1 surface expression in the tumor (Figure 6a), which suggested to us that combinational therapy targeting both UBR5 and PD-L1 may produce an additive or synergistic therapeutic benefit compared to either treatment alone. We tested the idea by targeting UBR5 expression with an shRNA and PD-L1 activity by a PD-L1 blocking antibody. The dual

Table 1. Upregulated proteins in *Ubr5*^{-/-} 4T1 tumor.

| Protein Names | Gene Names | 4T1/GFP Intensity | 4T1/ <i>Ubr5</i> ^{-/-} Intensity | 4T1/ <i>Ubr5</i> ^{-/-} /4T1/GFP (log2) | P value |
|--|------------|-------------------|---|---|----------|
| Fanconi anemia group A protein homolog | Fanca | 69.75 | 252.92 | 1.447440593 | 3.19E-09 |
| Retinoic acid early-inducible protein 1-delta | Raet1e | 313.1 | 1043.5 | 1.325759778 | 7.87E-08 |
| Alkaline phosphatase | Alpl | 1170.5 | 3749.2 | 1.268482444 | 2.95E-07 |
| Zinc finger protein 217 | Zfp217 | 135.55 | 410.37 | 1.187124744 | 2.01E-06 |
| Arsenite methyltransferase | As3mt | 356.33 | 1023.6 | 1.111390787 | 1.39E-05 |
| WAP four-disulfide core domain protein 2 | Wfdc2 | 24392 | 69426 | 1.098092588 | 1.79E-05 |
| Immunoglobulin superfamily member 8 | Igsf8 | 693.95 | 1873.9 | 1.022164933 | 9.38E-05 |
| Doublesex- and mab-3-related transcription factor A2 | Dmrta2 | 190.98 | 505.51 | 0.99334266 | 0.000154 |
| Claudin | Cldn3 | 93.988 | 246.53 | 0.980239332 | 0.000198 |
| Histone acetyltransferase | Kat7 | 1304.6 | 3282.6 | 0.920256019 | 0.000692 |
| Protein transport protein Sec61 subunit beta | Sec61b | 2392.7 | 5997.6 | 0.914770377 | 0.00074 |
| Caspase-1 | Casp1 | 428.37 | 1066.5 | 0.904979204 | 0.000809 |
| NEDD8-conjugating enzyme UBE2 F | Ube2 f | 593.58 | 1477.6 | 0.904765974 | 0.000809 |
| Cyclin-dependent kinase 13 | Cdk13 | 434.88 | 1008.3 | 0.802260273 | 0.005354 |
| Parafibromin | Cdc73 | 10257 | 23477 | 0.783663828 | 0.007422 |
| Bromodomain PHD Finger Transcription Factor | Bptf | 134.89 | 307.12 | 0.776043657 | 0.008314 |
| Deoxycytidylate deaminase | Dctd | 2655.2 | 5842.2 | 0.726715804 | 0.016953 |
| Retinol-binding protein 1 | Rbp1 | 6448.4 | 14172 | 0.725054818 | 0.017028 |
| ATP-dependent RNA helicase Dhx29 | Dhx29 | 129.66 | 282.6 | 0.713052578 | 0.020075 |
| Ubiquitin-conjugating enzyme E2 J1 | Ube2j1 | 368.29 | 795.18 | 0.699463837 | 0.024876 |
| Signal peptidase complex catalytic subunit SEC11 C | Sec11 c | 1243.1 | 2666.1 | 0.689813127 | 0.026887 |
| Ephrin type-A receptor 2 | Epha2 | 15419 | 32855 | 0.680428331 | 0.03027 |
| DDB1- and CUL4-associated factor 5 | Dcaf5 | 560.67 | 1190.9 | 0.675853084 | 0.031116 |
| Triple functional domain protein | Trio | 410.74 | 868.43 | 0.669208704 | 0.033234 |
| Heterogeneous nuclear ribonucleoprotein D0 | Hnrnpd | 9061.3 | 19054 | 0.661328535 | 0.03649 |
| Cytosolic phospholipase A2 | Pla2g4a | 6561 | 13739 | 0.655313965 | 0.03901 |
| UBX domain-containing protein 4 | Ubxn4 | 547.23 | 1145.8 | 0.655160605 | 0.03901 |
| Polyglutamine-binding protein 1 | Pqbp1 | 11115 | 23233 | 0.652692099 | 0.039935 |
| Guanine nucleotide-binding protein-like 3-like protein | Gnl3 l | 3221.1 | 6705.7 | 0.646859082666 | 0.043196 |
| Protein MANBAL | Manbal | 42.449 | 87.822 | 0.637876413 | 0.047799 |

LC/MS/MS analysis of differential protein expression. Proteins were extracted from 4T1/GFP and 4T1/*Ubr5*^{-/-} cells and labeled with TMT after digestion. The two samples were combined and analyzed by LC-MS/MS. Proteins were identified by searching database, and the data was analyzed by in-house R script. In total, 4,305 proteins were identified and 3644 of them were quantified. Compared to WT, 30 proteins were up-regulated in *Ubr5*^{-/-} cells with significant *p* values (*P* < 0.05)

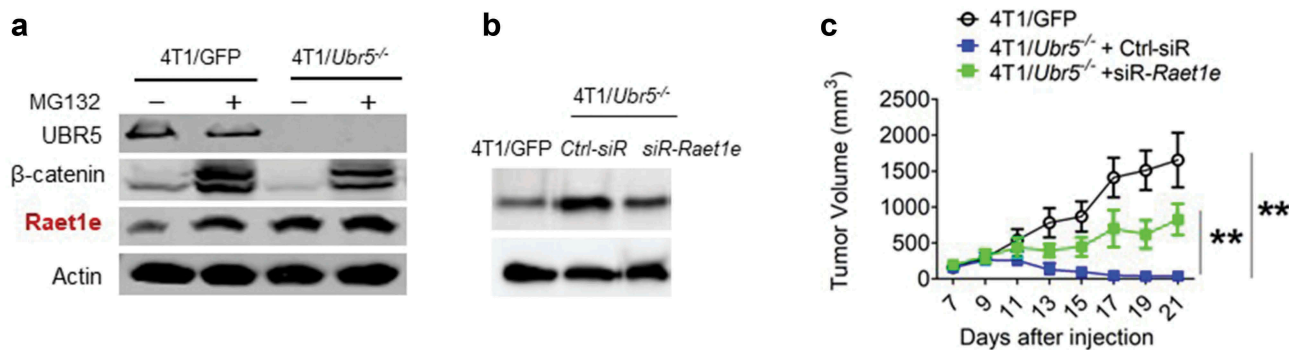


Figure 5. Potential immunogens and interacting partners controlled by UBR5. (a) Protein expression of Raet1e in WT vs. *Ubr5*^{-/-} 4T1 cells treated with MG132 or not, by Western blot analysis. (b,c) Knocking down Raet1e using siRNA in 4T1/*Ubr5*^{-/-} cells partially restored its tumor growth *in vivo*. (b) 48 h after siRNA transfection, Raet1e protein levels in 4T1 cells were measured by western blot. (c) After *Raet1e*-siRNA transfection, 4T1/*Ubr5*^{-/-} tumor cells were *s.c.* injected in the abdominal mammary gland. Tumor growth was monitored for 3 weeks. Data are representative of two independent experiments with similar results. Data represent mean \pm SEM, ***P* < .01.

targeting yielded superior therapeutic benefits than either treatment alone with respect to tumor size (Figure 6b). The targeting efficiency was evidenced via immunohistochemical (IHC) analysis by the diminished protein expression levels of UBR5 and PD-L1 in treated tumors, and the lowest level of both UBR5 and PD-L1 was presented in the tumor tissues with the interference of both UBR5 and PD-L1 compared to the control group (Figure 6c). Consistently with the drastically impaired tumor growth, dual targeting of UBR5 and PD-L1 resulted in dramatically reduced lung metastasis than mono-targeting (Figure 6d,e), and significantly extended survival (Figure 6f). These data demonstrate the therapeutic superiority of the combinational targeting strategy.

Discussion

An ingenuity pathway analysis (IPA)-based study that we performed (unpublished data) reveals that UBR5 may represent a major signaling hub connecting with many important molecules in various ways such as TP53, argonaute 1 (AGO1), Bcl-2-associated X protein (BAX), calcium and integrin binding 1 (CIB1), growth arrest and DNA damage-inducible 45 (GADD45) proto-oncogene MDM2, poly(A)-binding and interacting protein 2 (PAIP2), progesterone receptor (PGR), protein phosphatase 2 regulatory subunit Balpha (PPP2R2A), and AGTRI, etc., suggesting a broad network of biological pathways regulated by UBR5 through direct or indirect physical interactions. In this study, we present evidence that

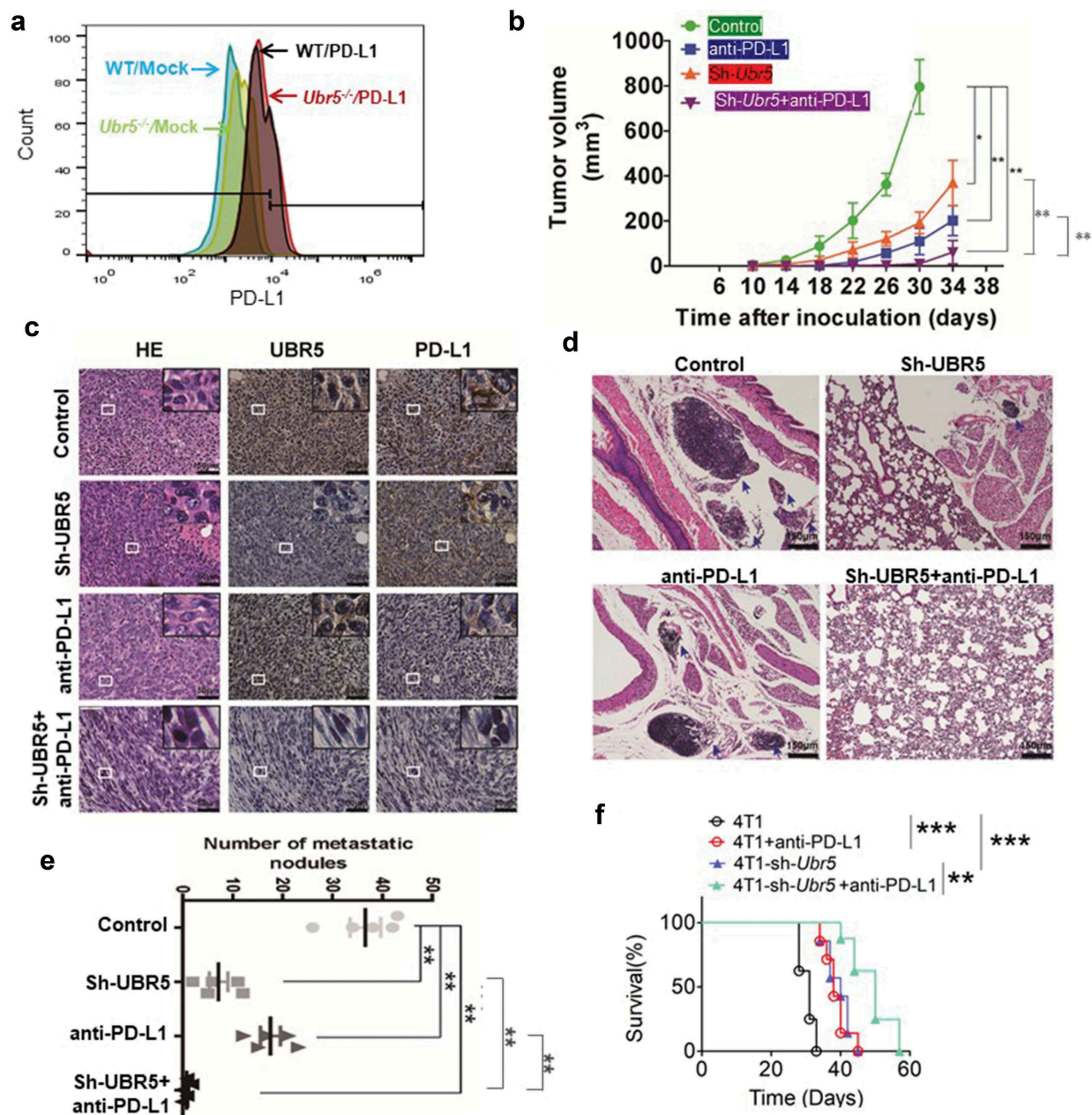


Figure 6. Combinational therapy targeting UBR5 and PD-L1. (a) FACS analysis of surface expression of PD-L1 on WT and *Ubr5*^{-/-} 4T1 cells. (b) Combination therapy targeting UBR5 (via shRNA) and PD-L1 (via antibody) in 4T1 tumors showing tumor growth. PD-L1 antibody (Bioxcell, clone 10 F.9G2) or isotype IgG (Rat IgG2b, κ) was injected intraperitoneally at 200 μg per mouse weekly since d 7 after tumor inoculation for 3 times in total. (c) Representative H&E staining and IHC staining of UBR5 and PD-L1 in WT 4T1 tumor tissues of indicated groups (scale bar = 50 μm). (d) Metastasis of the four treated groups illustrated by H&E staining of tumor tissues (d) and by quantifying metastatic nodules in the lungs (e). (f) Survival rate of mice with WT or *Ubr5*-deficient tumors treated with anti-PD-L1. Three different replicates were performed for all experiments. Data represent mean ± SEM; **P* < .05; ***P* < .01.

UBR5 gene amplifications are common occurrence in human breast cancers and that high *UBR5* expression is adversely associated with disease progression and patient survival. Targeting *UBR5* in the mammary tumor through gene editing or expression silencing causes paracrine effects that trigger the activation of CD8⁺ T cells, which help control the tumor growth. The antigenic specificities of this response are presently unknown. We have shown that Rael1e expression was upregulated in *Ubr5*^{-/-} tumor, which may stimulate an anti-tumor response. This response is unlikely to be of NK cell origin since depletion of NK cells did not have an impact on

the anti-tumor response (data not shown). It remains to be determined if γδ T cells are involved.¹⁸ Given *UBR5*'s demonstrated essential role for G(1)/S and intra S phase DNA damage checkpoint activation and for the maintenance of G(2)/M arrest and genome integrity after double-strand DNA breaks,²¹ it is conceivable that deletion of *Ubr5* may cause genomic instability and the induction of "neoantigens" that attract T cell-mediated immune responses. Further studies in this area may lead to the identification of these neoantigens for potential applications as novel cancer vaccine and immunotherapy targets.

In contrast to the strong paracrine involvement of CD8⁺ T-mediated immunity in UBR5-regulated tumor growth, the metastatic process driven by UBR5 appears to be primarily cell-intrinsic. Our data demonstrate that the annulling of *Ubr5* in 4T1 cells is causative for the loss of E-cadherin expression and impairs the tumor cells' mesenchymal to epithelial transition (MET) and their ability to colonize in secondary organs. This effect is controlled by UBR5 principally through transcriptional regulation of the key EMT regulators ID1 and ID3. The result is the maintenance of *Ubr5*^{-/-} tumor cells in the mesenchymal state lacking E-cadherin expression, thus unable to complete MET and take roots in the lungs. It is thus of great importance to further understand how UBR5 loss leads to ID1/ID3 downregulation. Given the mechanism of UBR5's action, it is possible that loss of UBR5 may lead to the stabilization of a repressor which inhibits ID1/ID3 expression. ATF3 is a well-characterized, known repressor of ID1 expression.²⁴ It will be interesting to determine if UBR5 destabilizes ATF3. It is equally possible that loss of UBR5 leads indirectly to the loss of a positively acting transcription factor that controls ID1/ID3 expression. A variety of factors that control ID1 expression in TNBC cells have been identified. The basic helix-loop-helix (bHLH) transcription factor Lyl1 and CREB1, a widely expressed transcription factor, and a suspected oncogene, interact and form a molecular complex. The histone acetyltransferases p300 and CBP are recruited to this complex. Together they activate CREB1 target promoters such as Id1, Id3, cyclin D3, Brca1, Btg2, and Egr1.²⁵

In summary, our findings may lead to the development of groundbreaking therapeutic modalities that, when combined with conventional treatment, will bring us significantly closer to ameliorating the immense casualty caused by highly aggressive breast cancer because targeting UBR5-mediated signaling pathway will not only bring immediate clinical benefits to patients by abrogating cancer growth and metastasis but may also lead to immune activation that will likely result in the generation of T cell memories and delicate immunosurveillance against cancer recurrence and drug resistance.

Highlights

- (1) We identify a profound role of UBR5 in breast cancer aggression.
- (2) Loss of UBR5 in cancer cells causes the appearance of certain putative immunogens.
- (3) Loss of UBR5 in cancer cells causes a strong CD8⁺ T cell-mediated anti-tumor response in a paracrine manner.
- (4) Loss of UBR5 in cancer cells severely impairs metastasis in a cell-intrinsic manner that is dependent on EMT regulators ID1 and ID3.
- (5) Combinational targeting of UBR5 and PD-L1 yields strong therapeutic benefit to tumor-bearing hosts.
- (6) The work significantly expands our scarce understanding of the pathophysiology and immunobiology of a fundamental molecule and has strong implications for the development of novel immunotherapy to treat aggressive breast cancers that resist conventional treatment.

Disclosure of potential conflicts of interest

No potential conflicts of interest were disclosed.

Funding

This work was supported in part by an NIH award (R03CA230573 to X. M.); by an award from the Emerson Collective Cancer Research Fund (ECCRF 191684 to X.M.); By an award from the Qatar National Research Foundation (NPRP-7-136-3-031 to L.C. and X.M.); By an award from the National Cancer Institute (PO1 CA094060 to R.B.) and support from The Breast Cancer Research Foundation to R.B.; by an award from the National Natural Science Foundation of China (81772747 to X.C.); by an award from the Shanghai Medical Guidance (Chinese and Western Medicine) Science and Technology Support Project (17411960200 to X. C.); by an award from the Clinical Peak Discipline Construction Project of Pudong New Area Government (PWYgf2018-03 to X.C.); by an award from the National Natural Science Foundation of China (81773154, 81974391 to C.W.); by an award from Pudong New Area Science and Technology Development Special Fund for People's Livelihood Research (PKJ2019-Y19 to C.W.).

Author contributions

M.S., C.W., X.C., and X.M.: contributed to study concept and design, analysis, and interpretation of data, writing of the manuscript, statistical analysis, obtained funding, study supervision. H.W.: performed meta-analysis of clinical data; T.Z.: performed bioinformatic analysis of the RNA-seq data; J.L. made the Rael1e mutants; R.B.: guided the metastasis experiments; L.C.: contributed human clinical samples. All authors read and approved the final manuscript.

ORCID

Tuo Zhang  <http://orcid.org/0000-0001-5396-918X>

References

1. R L S, Miller KD, Jemal A. Cancer statistics, 2015. *CA Cancer J Clin.* 2015;65:5–29. doi:10.3322/caac.21254.
2. Liao L, Song M, Li X, Tang L, Zhang T, Zhang L, Pan Y, Chouchane L, Ma X. E3 ubiquitin ligase UBR5 drives the growth and metastasis of triple negative breast cancer. *Cancer Res.* 2017;77:2090–2101. doi:10.1158/0008-5472.CAN-16-2409.
3. M J C, Russell AJ, Woollatt E, Sutherland GR, Sutherland RL, Watts CK. Identification of a human HECT family protein with homology to the Drosophila tumor suppressor gene hyperplastic discs. *Oncogene.* 1998;17:3479–3491. doi:10.1038/sj.onc.1202249.
4. D N S, Hird SL, Withington SL, Dunwoodie SL, Henderson MJ, Biben C, Sutherland RL, Ormandy CJ, Watts CK. Edd, the murine hyperplastic disc gene, is essential for yolk sac vascularization and chorioallantoic fusion. *Mol Cell Biol.* 2004;24:7225–7234. doi:10.1128/MCB.24.16.7225-7234.2004.
5. Kinsella E, Dora N, Mellis D, Lettice L, Deveney P, Hill R, Ditzel M. Use of a conditional *Ubr5* mutant allele to investigate the role of an N-end rule ubiquitin-protein ligase in hedgehog signalling and embryonic limb development. *PLoS One.* 2016;11:e0157079. doi:10.1371/journal.pone.0157079.
6. R F S, Frikstad KM, McKenna J, McCloy RA, Deng N, Burgess A, Stokke T, Patzke S, Saunders DN. The E3 ubiquitin ligase UBR5 regulates centriolar satellite stability and primary cilia. *Mol Biol Cell.* 2018;mbcE17040248. doi:10.1091/mbc.E17-04-0248.
7. Koyuncu S, Saez I, Lee HJ, Gutierrez-Garcia R, Pokrzywa W, Fatima A, Hoppe T, Vilchez D. The ubiquitin ligase UBR5 suppresses proteostasis collapse in pluripotent stem cells from Huntington's disease patients. *Nat Commun.* 2018;9:2886. doi:10.1038/s41467-018-05320-3.

8. J L C, Henderson MJ, Russell AJ, Anderson DW, Bova RJ, Campbell IG, Choong DY, Macdonald GA, Mann GJ, Nolan T, et al. EDD, the human orthologue of the hyperplastic discs tumour suppressor gene, is amplified and overexpressed in cancer. *Oncogene*. 2003;22:5070–5081. doi:10.1038/sj.onc.1206775.
9. D R R, Wu YM, Lonigro RJ, Vats P, Cobain E, Everett J, Cao X, Rabban E, Kumar-Sinha C, Raymond V, et al. Integrative clinical genomics of metastatic cancer. *Nature*. 2017;548:297–303. doi:10.1038/nature23306.
10. D S C, Bashel B, Balasubramanya SAH, Creighton CJ, Ponce-Rodriguez I, Chakravarthi B, UALCAN: VS. A portal for facilitating tumor subgroup gene expression and survival analyses. *Neoplasia* (New York, NY). 2017;19:649–658. doi:10.1016/j.neo.2017.05.002.
11. Liu J, Lichtenberg T, Hoadley KA, Poisson LM, Lazar AJ, Cherniack AD, Kovatich AJ, Benz CC, Levine DA, Lee AV, et al. An integrated TCGA Pan-cancer clinical data resource to drive high-quality survival outcome analytics. *Cell*. 2018;173:400–416. e411. doi:10.1016/j.cell.2018.02.052.
12. Dobin A, Davis CA, Schlesinger F, Drenkow J, Zaleski C, Jha S, Batut P, Chaisson M, Gingeras TR. STAR: ultrafast universal RNA-seq aligner. *Bioinformatics*. 2013;29:15–21. doi:10.1093/bioinformatics/bts635.
13. Anders S, Pyl PT, Huber W. HTSeq—a Python framework to work with high-throughput sequencing data. *Bioinformatics*. 2015;31:166–169. doi:10.1093/bioinformatics/btu638.
14. M I L, Huber W, Anders S. Moderated estimation of fold change and dispersion for RNA-seq data with DESeq2. *Genome Biol*. 2014;15:550. doi:10.1186/s13059-014-0550-8.
15. Kramer A, Green J, Pollard J Jr., Tugendreich S. Causal analysis approaches in ingenuity pathway analysis. *Bioinformatics*. 2014;30:523–530. doi:10.1093/bioinformatics/btt703.
16. Dompe N, Rivers CS, Li L, Cordes S, Schwickart M, Punnoose EA, Amler L, Seshagiri S, Tang J, Modrusan Z, et al. A whole-genome RNAi screen identifies an 8q22 gene cluster that inhibits death receptor-mediated apoptosis. *Proc Natl Acad Sci U S A*. 2011;108:E943–951. doi:10.1073/pnas.1100132108.
17. Stankic M, Pavlovic S, Chin Y, Brogi E, Padua D, Norton L, Massague J, Benezra R. TGF-beta-Id1 signaling opposes Twist1 and promotes metastatic colonization via a mesenchymal-to-epithelial transition. *Cell Rep*. 2013;5:1228–1242. doi:10.1016/j.celrep.2013.11.014.
18. Kong Y, Cao W, Xi X, Ma C, Cui L, He W. The NKG2D ligand ULBP4 binds to TCRgamma9/delta2 and induces cytotoxicity to tumor cells through both TCRgammadelta and NKG2D. *Blood*. 2009;114:310–317. doi:10.1182/blood-2008-12-196287.
19. Xu Y, Zhou L, Zong J, Ye Y, Chen G, Chen Y, Liao X, Guo Q, Qiu S, Lin S, et al. Decreased expression of the NKG2D ligand ULBP4 may be an indicator of poor prognosis in patients with nasopharyngeal carcinoma. *Oncotarget*. 2017;8:42007–42019. doi:10.18632/oncotarget.14917.
20. Cho H, Chung JY, Kim S, Braunschweig T, Kang TH, Kim J, Chung EJ, Hewitt SM, Kim JH. MICA/B and ULBP1 NKG2D ligands are independent predictors of good prognosis in cervical cancer. *BMC Cancer*. 2014;14:957. doi:10.1186/1471-2407-14-957.
21. M A M, Saunders DN, Henderson MJ, Clancy JL, Russell AJ, Lehrbach G, Musgrove EA, Watts CK, Sutherland RL. The E3 ubiquitin ligase EDD regulates S-phase and G(2)/M DNA damage checkpoints. *Cell Cycle*. 2007;6:3070–3077. doi:10.4161/cc.6.24.5021.
22. Smits VA. EDD induces cell cycle arrest by increasing p53 levels. *Cell Cycle*. 2012;11:715–720. doi:10.4161/cc.11.4.19154.
23. Ling S, Lin WC. EDD inhibits ATM-mediated phosphorylation of p53. *J Biol Chem*. 2011;286:14972–14982. doi:10.1074/jbc.M110.182527.
24. Li J, Yang Z, Chen Z, Bao Y, Zhang H, Fang X, Yang W. ATF3 suppresses ESCC via downregulation of ID1. *Oncol Lett*. 2016;12:1642–1648. doi:10.3892/ol.2016.4832.
25. San-Marina S, Han Y, Suarez Saiz F, Trus MR, Minden MD. Lyl1 interacts with CREB1 and alters expression of CREB1 target genes. *Biochim Biophys Acta*. 2008;1783:503–517. doi:10.1016/j.bbamcr.2007.11.015.